

## Adaptive Poly - FEM for the analysis of plane elasticity problems

Balaji Kasi, Amirtham Rajagopal & Paul Steinmann

To cite this article: Balaji Kasi, Amirtham Rajagopal & Paul Steinmann (2017): Adaptive Poly - FEM for the analysis of plane elasticity problems, International Journal for Computational Methods in Engineering Science and Mechanics, DOI: [10.1080/15502287.2017.1301596](https://doi.org/10.1080/15502287.2017.1301596)

To link to this article: <http://dx.doi.org/10.1080/15502287.2017.1301596>



Accepted author version posted online: 13 Apr 2017.



Submit your article to this journal [↗](#)



Article views: 13



View related articles [↗](#)



View Crossmark data [↗](#)

Adaptive Poly - FEM for the analysis of plane elasticity problems

Balaji Kasi<sup>1</sup>, Amirtham Rajagopal\*<sup>1</sup> and Paul Steinmann<sup>2</sup>

<sup>1</sup>Department of Civil Engineering, Indian Institute of Technology Hyderabad, A.P, India.

<sup>2</sup>Chair of Applied Mechanics, University of Erlangen, Nuremberg, Germany.

### Abstract

In this work we present an adaptive polygonal finite element method (Poly-FEM) for the analysis of two dimensional plane elasticity problems. The generation of meshes consisting of  $n$ -sided polygonal finite elements is based on the generation of a centroidal Voronoi tessellation (CVT). An unstructured tessellation of a scattered point set, that minimally covers the proximal space around each point in the point set is generated whereby the method also includes tessellation of non-convex domains. In this work we propose a region by region adaptive polygonal element mesh generation. A patch recovery type of stress smoothing technique that utilizes polygonal element patches for obtaining smooth stresses is proposed for obtaining the smoothed finite element stresses. A recovery type *a-posteriori* error estimator that estimates the energy norm of the error from the recovered solution is then adopted for the polygonal finite element method. The refinement of the polygonal elements is then made on a region by region basis through a refinement index. For the numerical integration of the Galerkin weak form over polygonal finite element domains we resort to classical Gaussian quadrature applied to triangular sub domains of each polygonal element. Numerical examples of two dimensional plane elasticity problems are presented to demonstrate the efficiency of the proposed adaptive polygonal finite element method.

**Keywords:** Polygonal finite elements, *a-posteriori* error estimator, adaptive finite element analysis.

## 1 Introduction

The finite element method is a powerful numerical tool for solving partial differential equations. The use of two dimensional triangular or quadrilateral elements and three dimensional tetrahedral or hexahedral elements is the popular standard case. However, there are associated complexities such as developing robust and fast algorithms for generating quality meshes on two or three dimensional complex geometries of micro structures, distortion effects under large deformation, complexities in development and use of higher order elements and the need for efficient quadrature schemes for the evaluation of integrals, amongst others. The use of polygonal elements with  $n$ - number of sides will provide greater flexibility and better accuracy to address some of these problems. Polygonal finite element discretizations can be useful in many areas like, e.g. the nonlinear constitutive modeling of polycrystalline materials with general anisotropic or ferroelectric [1, 2] behavior where each grain is represented with its independent properties by one element, for interface elements connecting dissimilar finite element meshes [3], for two field methods solving diffusion equations [4], for solid mechanics problems [5] including incompressible materials [6], and for topology optimization [7]. The recent focus in polygonal FEM has also been on generating conformal polygonal discretizations [8–10], developing numerical integration schemes for polygonal finite element methods either based on conformal mapping [11, 12] or generalizing Gaussian quadrature rules [13, 14], and the natural element method for non-convex and discontinuous problems [15]. Constantiniu et al. [16] recently developed the adaptive Delaunay tessellation, which is an extremely useful method for generating unique polygonal

---

\*Corresponding author email: rajagopal@iith.ac.in

tessellations. The method has been extended by Kraus et al. [10] to include non-convex domains and conformal interpolation techniques on polygons for solving elasticity problems.

Recent works on polygonal finite element methods include: Sukumar et al. [17] established the connections between the virtual element method (VEM) and hourglass control techniques and showed quantitative comparisons of the consistency and stabilization matrices in the VEM to those in the hourglass control method. Heng et al. [18] have given an approach towards the challenging task of modeling nonlinear elastic materials with standard finite elements and have proposed an alternative approach to model finite elasticity problems in two dimensions by using polygonal discretizations. Gianmarco et al. [19] worked on the new perspectives on polygonal and polyhedral finite element methods. Floater et al. [20] have discussed on gradient bounds for Wachspress coordinates on polytopes. An approach regarding polygonal finite elements approximation for mixed formulations was given by Cameron et al. [21] for incompressible fluid flow. It has been demonstrated that a certain class of approximants can be devoid of spurious modes and locking. Cameron et al. [7] proposed a polygonal finite element procedure for topology optimization. In another recent work [21] integration errors in polygonal finite element methods and its relevance from the perspective of the patch test have been discussed. Arun et al. [22] proposed the Virtual Element Method (VEM) for the numerical solution of boundary value problems on arbitrary polyhedral meshes and also presented several numerical studies in order to verify convergence of the VEM and evaluate its performance for various types of meshes. Khoei et al. [23] presented a polygonal-FEM technique for the modeling of arbitrary interfaces in large deformations and applied it to capture discontinuous deformations in the non-conformal elements, which are cut by the interface in a uniform regular mesh. Biabanaki et al. [24] presented a polygonal finite element method for large deformation frictionless dynamic contact-impact problems with non-conformal meshes. Sukumar et al. [25] presented the development of quadratic serendipity shape functions on planar convex and nonconvex polygons and maximized the objective functional subject to the constraints for quadratic completeness. A numerical algorithm based on group theory and numerical optimization was presented by Mousavi et al. [14] to compute efficient quadrature rules for integration of bivariate polynomials over arbitrary polygons. The algorithm was used for the construction of symmetric and non-symmetric quadrature rules over convex and concave polygons. Nguyen et al. [26] provided an approach towards free and forced vibration analysis using the  $n$ -sided polygonal cell-based smoothed finite element method. They further extended the nCS-FEM to the free and forced vibration analyses of two dimensional dynamic problems. Hornmann et al. [27] introduced a new generalization of barycentric coordinates that stems from the maximum entropy principles. David et al. [28] presented a mixed-element mesh generator based on the modified octree approach that has been adapted to generate polyhedral Delaunay meshes. Yijiang et al. [29] presented an explicit expression of the two-dimensional element compliance matrix on the complementary energy principle with concave polygonal meshes. Dai et al. [6] proposed a smoothed finite element method (SFEM) using quadrilateral elements, thus the method produces very accurate stresses and desirable convergence rate as compared with FEM. Kraus and Steinmann [30] presented finite element formulations for 3D convex polyhedra in nonlinear continuum mechanics. An  $n$ -sided polygonal edge based smoothed finite element method (nES-FEM) for solid mechanics problems is discussed in [9]. Somnath et al. [31] developed a Voronoi cell finite element method to solve small deformation elastic-plastic problems for arbitrary heterogeneous materials and conducted studies to understand the effect of size, shape and distribution of a second phase on the averaged and true local responses of representative material elements. Zhang et al. [32] developed a parametric variational principle based polygonal finite element method (PFEM) and Voronoi cell finite element method (VCFEM) for numerical simulations of the elastic-plastic mechanical behavior of heterogeneous materials under small deformation and also gave the shape functions for the polygonal element. Sundararajan et al. [33] studied the convergence and accuracy of displacement based finite element formulations over arbitrary polygons. Laplace interpolants, strain smoothing and scaled boundary polygon formulation was considered for the analysis. Andrew et al. [34] studied error estimates for generalized barycentric interpolation. An efficient numerical scheme for the biharmonic equation by weak Galerkin finite element methods on polygonal or polyhedral meshes has been made in [35]. Higher order BEM-based FEM on polygonal meshes have been studied recently (see [36] and [37]).

The quality of finite element solutions is not equally good in all regions of the domain under consid-

eration, thus making a locally finer mesh necessary. The general recognition is that a reliable numerical approximation of the analytical solution of a given mathematical model needs the notion of discretization errors with bounds. Initial contributions in this regard can be attributed to Babuska et al. [38] and further works by Babuska and Rheinboldt [39], presenting a priori error estimators in the energy norm for second-order adjoint elliptic boundary value problems. The breakthrough in error-controlled adaptivity of primal finite element methods (the displacement approach) was achieved by Babuska and Miller [40], presenting the *a - posteriori* error analysis of the discretization error for second-order elliptic problems in the global energy norm with bounds from below and from above. Zienkiewicz and Zhu [41] presented an *a - posteriori* super convergent patch recovery based error indicator [42] using explicitly calculated smoothed stresses, assuming that the smoothed stresses are more accurate than the discretized ones [43]. This methodology has been used as a basis for advanced adaptive strategies in some of the recent works [44–47]. A more detailed review on advances in error estimation strategies can be found in [48] and [49]. There has been recent work on adaptive singular finite element [50] and refinement strategies based on asymptotic expansions of finite element solutions [51]. The error estimates for generalized barycentric coordinates are discussed in [52]. Gonzalez et al. [53] recently presented a mesh adaptive strategy driven by goal oriented locally equilibrated super convergent patch recovery. These patch recovery techniques have also been used recently in numerical implementation of strain gradient plasticity [54].

In this work we present an adaptive polygonal finite element method for the analysis of two dimensional plane elasticity problems. The generation of polygonal finite element meshes is based on the centroidal Voronoi tessellation (CVT). By this method an unstructured tessellation of a scattered point set that minimally covers the proximal space around each point can be generated. The method has also been extended to include non-convex domains. For the numerical integration of the Galerkin weak form over polygonal finite element domains we resort to classical Gaussian quadrature applied to triangular sub domains of each polygonal element. An adaptive refinement strategy is proposed in the present work. A patch recovery type of stress smoothing technique that utilizes polygonal patches to obtain smooth stresses is proposed. A classical recovery type *a - posteriori* error estimator that estimates the energy norm of the error from the recovered solution is then implemented. The refinement of the polygonal elements is made on an element by element basis via a refinement index. Numerical examples of two dimensional plane elasticity problems are presented to demonstrate the efficiency of the proposed adaptive polygonal finite element method.

The outline of the paper is as follows : in Section 2, after a brief review of mathematical preliminaries we present an overview of generating the polygonal finite element mesh using CVT and details of the extension of the methodology to non-convex domains are presented. In Section 3 we discuss the non-polynomial type polygonal interpolant used in the present work. Section 4 presents equilibrium equations, weak form and discretized weak form for two dimensional plane elasticity problems. A numerical integration strategy performed by dividing the polygonal domain into triangular subdomains and then using well known quadrature rules on a triangle is presented in Section 5. Section 6 presents the details of *a-posteriori* error estimates and adaptive refinement. In the last Section 7, we present numerical examples of plane elasticity problems and study the convergence characteristics under uniform and adaptive mesh refinement.

## 2 Polygonal finite element discretization

In this section we present a simple and robust method for polygonal mesh generation. The main components of a mesh generator are an implicit description of the domain geometry and the centroidal Voronoi tessellation (CVT) [55] used for its discretization. The signed distance function contains all the essential information about the domain geometry and offers great flexibility to construct a relatively large class of domains. Lloyd’s method is used to ensure uniform (optimal) distribution of seeds and thus a high quality mesh (Talischi et al. [7]). Examples are provided to illustrate capabilities of the proposed discretization methodology.

## 2.1 Signed distance function and implicit representation

Let  $\Omega$  be a subset of  $\mathbb{R}^2$ . The *signed distance function* associated with  $\Omega$  is defined by

$$d_{\Omega}(\mathbf{X}) = S_{\Omega}(\mathbf{X}) \min_{\mathbf{Y} \in \partial\Omega} \|\mathbf{X} - \mathbf{Y}\| \quad (1)$$

where  $\partial\Omega$  denotes the boundary of  $\Omega$ .  $\|\cdot\|$  is the standard Euclidean norm in  $\mathbb{R}^2$ . Here  $\|\mathbf{X} - \mathbf{Y}\|$  is the distance between any point  $\mathbf{X}$  and point  $\mathbf{Y}$  on the boundary of domain, and the sign function is given by

$$S_{\Omega}(\mathbf{X}) := \begin{cases} -1, & \text{if } \mathbf{X} \in \Omega \\ +1, & \text{if } \mathbf{X} \in \mathbb{R}^2 \setminus \Omega \end{cases}$$

Thus, if  $\mathbf{X}$  lies inside the domain  $\Omega$ ,  $d_{\Omega}(\mathbf{X})$  is minus the distance of  $\mathbf{X}$  to the closest boundary point. The following characterizations are drawn from this definition

$$\Omega = \{\mathbf{X} \in \mathbb{R}^2 : d_{\Omega}(\mathbf{X}) \leq 0\} \quad (2)$$

$$\partial\Omega = \{\mathbf{X} \in \mathbb{R}^2 : d_{\Omega}(\mathbf{X}) = 0\} \quad (3)$$

$$\bar{\Omega} = \Omega \cup \partial\Omega \quad (4)$$

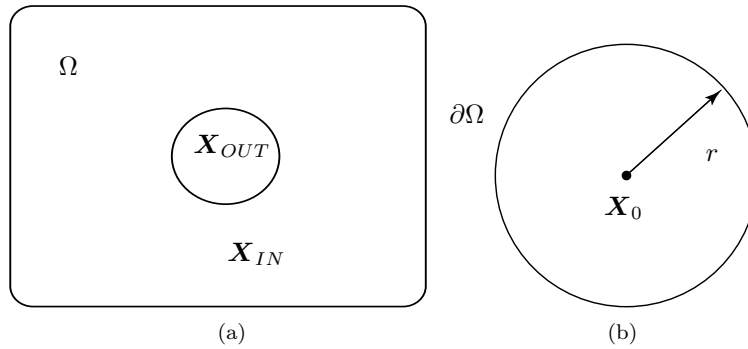


Figure 1: (a) For the domain above  $d_{\Omega}(\mathbf{X}_{IN}) < 0$  and  $d_{\Omega}(\mathbf{X}_{OUT}) > 0$ . (b) A circular domain of radius  $r$ .

For the domain shown in Fig. 1a, consider two points  $\mathbf{X}_{OUT}$  and  $\mathbf{X}_{IN}$  which are outside and inside the domain  $\Omega$ , respectively. Thus the distance function of point  $\mathbf{X}_{OUT}$  is positive,  $d_{\Omega}(\mathbf{X}_{OUT}) > 0$ , and that of  $\mathbf{X}_{IN}$  is negative,  $d_{\Omega}(\mathbf{X}_{IN}) < 0$ , implying that points  $\mathbf{X}_{OUT}$  and  $\mathbf{X}_{IN}$  are outside and inside the domain  $\Omega$ , respectively.

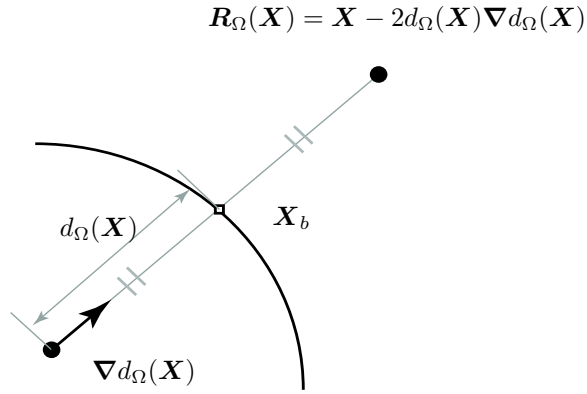
We can see from the discussion so far that when  $\Omega$  is characterized by its signed distance function information about  $\Omega$  can be readily extracted. The essential task then is to construct  $d_{\Omega}(\mathbf{X})$  for a given domain  $\Omega$  that we wish to discretize. For example, if  $\Omega$  is a circle of radius  $r$  centered at point  $\mathbf{X}_0$ , (See Fig.1b) the distance function for that domain is given by,

$$d_{\Omega}(\mathbf{X}) = \|\mathbf{X} - \mathbf{X}_0\| - r \quad (5)$$

Other useful information about the domain geometry given by the signed distance function is the direction of the nearest boundary point, given by its gradient  $\nabla d_{\Omega}(\mathbf{X})$ . We use the property of the gradient to find the reflection of any point  $\mathbf{X}$  about the closest boundary point. We denote the reflection by  $\mathbf{R}_{\Omega}(\mathbf{X})$ , see Fig. 2.

$$\mathbf{R}_{\Omega}(\mathbf{X}) = \mathbf{X} - 2d_{\Omega}(\mathbf{X})\nabla d_{\Omega}(\mathbf{X}) \quad (6)$$

This reflection property is used in the mesh generation to obtain a polygonal mesh confined to a defined geometry (Explained in Sec. 2.3).

Figure 2: Reflection of a point  $\mathbf{X}$  about nearest boundary point  $\mathbf{X}_b$ 

## 2.2 Centroidal Voronoi tessellation (CVT) and Lloyd's algorithm

Consider a set of nodes  $\mathcal{P} = \{\mathbf{P}_1, \mathbf{P}_2, \dots, \mathbf{P}_M\}$  with  $\mathbf{P}_I \in \mathbb{R}^2$ . The first order Voronoi diagram  $\mathcal{V}(\mathcal{P})$  of the set  $\mathcal{P}$  is a subdivision of the Euclidean space  $\mathbb{R}^2$  into convex regions

$$\mathcal{V}(\mathbf{P}_I) = \{\mathbf{x} \in \mathbb{R}^2 : \|\mathbf{P} - \mathbf{P}_I\| < \|\mathbf{P} - \mathbf{P}_J\| \forall J \neq I\}$$

called Voronoi cells, where  $\mathcal{V}(\mathcal{P}) = \cup \mathcal{V}(\mathbf{P}_I)$ , as shown in Fig.3.

The above definition states that any point  $\mathbf{x}$  in the Voronoi cell  $\mathcal{V}(\mathbf{P}_I)$  is closer to node  $\mathbf{P}_I$  than to any other node  $\mathbf{P}_J$ . The regularity of a Voronoi diagram is determined entirely by the distribution of the generating point set. A random set of generators may lead to a discretization not suitable for use in finite element analysis. Therefore, we restrict our attention to a special class of Voronoi tessellation that enjoys a higher level of regularity, i.e., centroidal Voronoi tessellation (CVT). A Voronoi tessellation is *centroidal* if for every  $\mathbf{P}_I \in \mathcal{P}$ ,  $\mathbf{P}_I = \mathbf{P}_c$  where,

$$\mathbf{P}_c = \frac{\int_{\mathcal{V}(\mathbf{P}_I)} \mathbf{x} \rho(\mathbf{x}) d\mathbf{x}}{\int_{\mathcal{V}(\mathbf{P}_I)} \rho(\mathbf{x}) d\mathbf{x}} \quad (7)$$

and  $\rho(\mathbf{x})$  is any given density function defined over  $\mathcal{V}(\mathbf{P}_I)$ . For a uniform distribution of points  $\rho(\mathbf{x}) = 1$ . Hence in a centroidal Voronoi tessellation (Voronoi diagram), the generating point of each Voronoi cell is

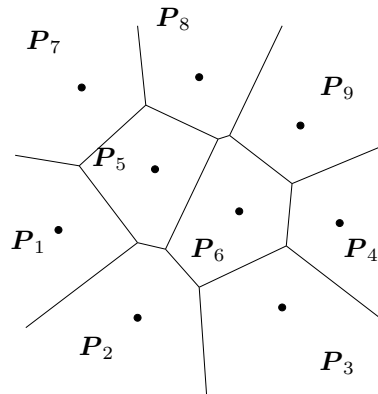


Figure 3: Voronoi diagram of a given point set.

also the centroid (center of mass) of the corresponding Voronoi region. It can be viewed as an optimal partition corresponding to an optimal distribution of generators. A number of algorithms are available to generate centroidal Voronoi tessellation. We adopt the simple and powerful *Lloyd's algorithm* for generating CVTs.

*Lloyd's algorithm*, also known as Voronoi iteration, is a deterministic algorithm for generating CVTs. It is an iterative process between computing Voronoi diagrams and mass centroids. It starts with an initial distribution of a point set which is iteratively replaced by centroids of corresponding Voronoi regions. Fig. 4 and Algorithm 1 sketch the procedure.

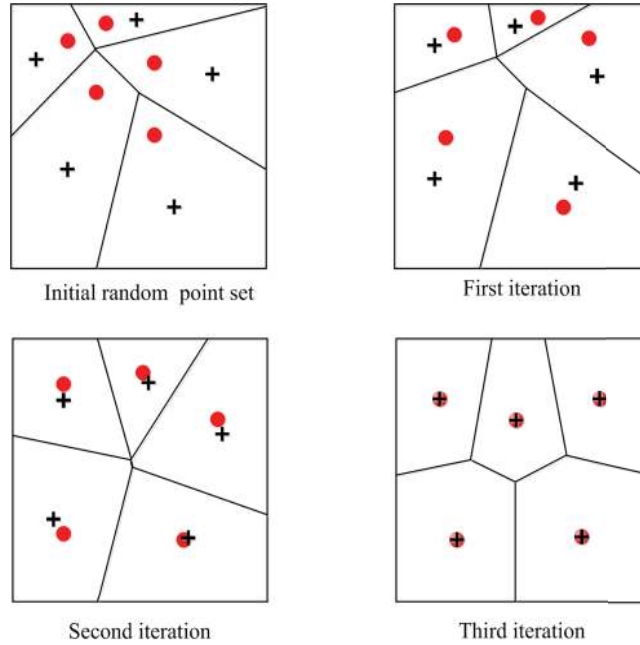


Figure 4: Lloyd's Algorithm : The Voronoi diagram of the current points at each iteration is shown. The  $\+$  sign denotes the centroids of the Voronoi cells.

---

**Algorithm 1** Lloyd's method

---

- 1: **Initialization**: Select an initial set of  $K$  points  $\{\mathbf{P}_I\}_{I=1}^K$ , represented as in Fig. 4.
  - 2: **Voronoi tessellation**: Construct the Voronoi sets  $\{\mathcal{V}\}$  associates with  $\{\mathbf{P}_I\}_{I=1}^K$
  - 3: **Centroid computation**: Determine the mass centroids (Eqn.(7)) of the Voronoi sets  $\mathcal{V}(\mathbf{P}_I)$  formed in Step 2. These centroids form a new set of points  $\{\bar{\mathbf{P}}_I\}_{I=1}^K$ , represented as  $\+$  sign in Fig. 4.
  - 4: **Convergence test**: If these new point set meets the convergence criterion  $\sum_{I=1}^K \|\bar{\mathbf{P}}_I - \mathbf{P}_I\| \leq TOL$ , terminate, else return to Step 2
- 

**2.3 Methodology to approximate the boundary**

Assume  $\Omega \subset \mathbb{R}^2$  is a bounded convex domain with smooth boundary and  $\mathcal{P}$  is a given set of distinct seeds in  $\Omega$ . To construct a polygonal discretization of  $\Omega$ , we first reflect all points in  $\mathcal{P}$  about the closest boundary point of  $\partial\Omega$  and denote the resulting set by  $R_\Omega(\mathcal{P})$

$$R_\Omega(\mathcal{P}) = \{R_\Omega(\mathbf{P}_I) : \mathbf{P}_I \in \mathcal{P}\} \tag{8}$$

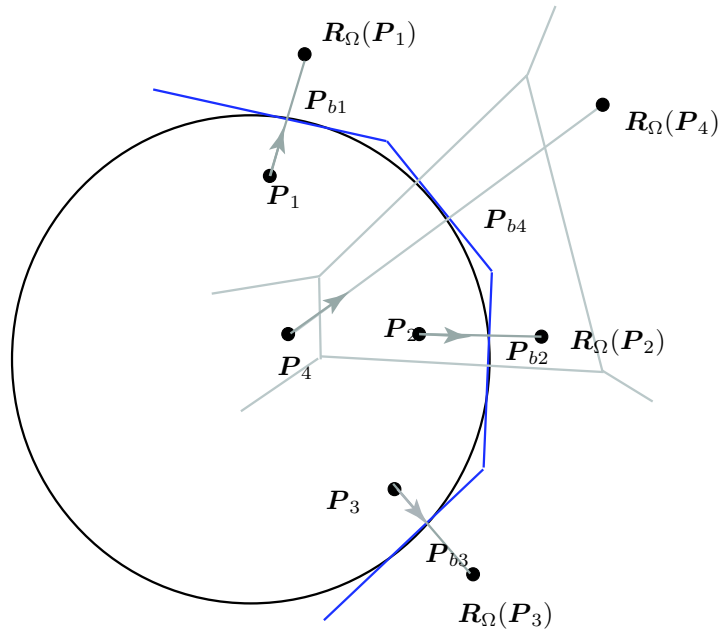


Figure 5: Voronoi edges shared between seeds and their reflection approximate the boundary of the domain. Reflection of interior seeds, say  $P_4$ , has no effect on tracing the boundary of the domain.

Convexity of  $\Omega$  ensures that all the reflected points lie outside  $\Omega$ . We then construct the Voronoi diagram of the original point set as well as its reflection. In other words, we compute  $\mathcal{V}(\mathcal{P} \cup R_{\Omega}(\mathcal{P}))$ . If Voronoi cells of a point  $P_I$  and its reflection have a common edge, i.e., if  $\mathcal{V}(P_I) \cap \mathcal{V}(R_{\Omega}(P_I)) \neq \emptyset$ , then this edge is tangent to  $\partial\Omega$  at  $P_{bI}$  as in Fig. 5. Therefore, these edges form an approximation to the domain boundary and a reasonable discretization of  $\Omega$  is given by the collection of Voronoi cells corresponding to the points in  $\mathcal{P}$ .

With this basic idea we can extend the procedure to more general domains, in particular those that are non-convex and have piecewise smooth boundaries (presence of corner points on  $\partial\Omega$ ). Fig. 6 shows the various arbitrary domains generated using the sketched algorithm.

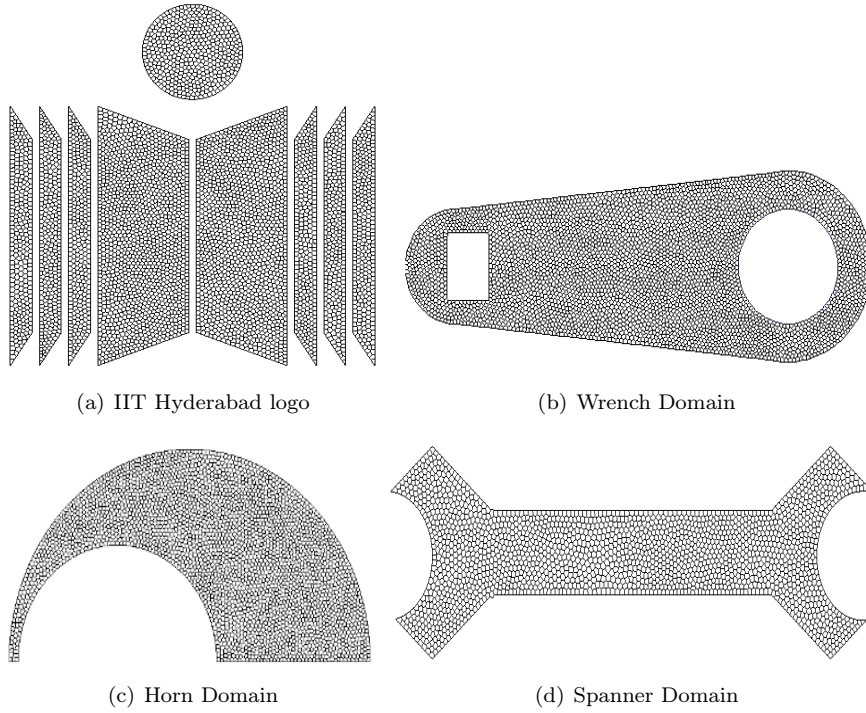


Figure 6: Sample polygonal meshes generated using the CVT procedure.

### 3 Conforming interpolants on polygons

Though there are many interpolants defined over polygonal domains, we prefer to use the Laplace interpolant in our analysis owing to its ease and simplicity. Consider a set of  $K$  nodes  $\mathbf{P}_I = (P_{Ix}, P_{Iy})$  in a domain  $\Omega \in \mathbb{R}^2$ . At any point  $\mathbf{P} = (P_x, P_y)$  inside  $\Omega$  or on its boundary  $\partial\Omega$  a set of associated interpolants  $\phi_I(\mathbf{P})$  is defined. Using this, an interpolation scheme for a scalar-valued function  $f(\mathbf{P})$  can be written as

$$f^h(\mathbf{P}) = \sum_{I=1}^N \Phi_I(\mathbf{P}) f_I \quad (9)$$

where  $f_I = f(\mathbf{P}_I)$  are the function values at the  $K$  nodes of the polygon. The function  $\Phi_I(\mathbf{P})$ , satisfies properties such as partition of unity, interpolation and linear completeness inside the polygon and on the boundaries. Various geometric measures like edge length, signed area, and sine or cosine of the angles at each vertex of the polygon are used to construct polygonal interpolants. The Laplace natural neighbor interpolant is the simplest and most popular Voronoi based interpolation method on polygonal domains [56–58]. The scheme, originally based on the concept of natural neighbors [59], is widely applicable for polygonal domains owing to its ease of implementation, and ability to account for a density distribution of nodes in a discretization. Fig.7 shows the Voronoi cells for an added point  $\mathbf{P}$  within a (canonical) polygonal domain with six nodes. The Laplace interpolation functions [57] are defined using the geometric properties of the Voronoi cell as

$$\phi_I^L(\mathbf{P}) = \frac{w_I(\mathbf{P})}{\sum_{J=1}^N w_J(\mathbf{P})} \quad (10)$$

$$w_I(\mathbf{P}) = \frac{s_I(\mathbf{P})}{h_I(\mathbf{P})} \quad (11)$$

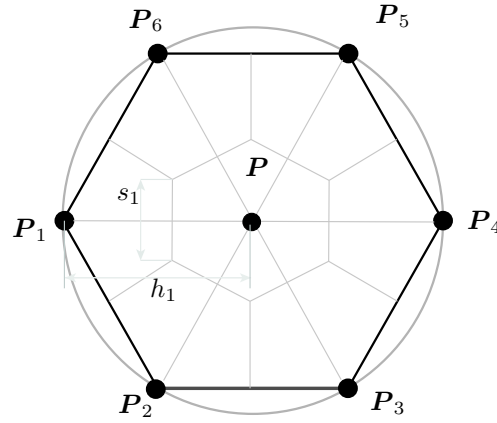


Figure 7: Voronoi based geometric measures for the Laplace interpolant: length of the associated Voronoi edge  $s_I$ , and the Euclidean distance  $h_I$  to the evaluation point  $P$ .

where  $s_I(P)$  is the length of the associated Voronoi edge and  $h_I(P) = \|P - P_I\|$  is the Euclidean distance from node  $P$  to node  $I$ , see Fig. 7. As only lengths of the Voronoi cells are taken into account, this method belongs to the class of non-Sibson interpolants. The Laplace interpolant  $\phi_I^L$  on a canonical domain  $\Omega_0$ , in which all nodes are regularly distributed on a unit circle, is shown in Fig. 8.

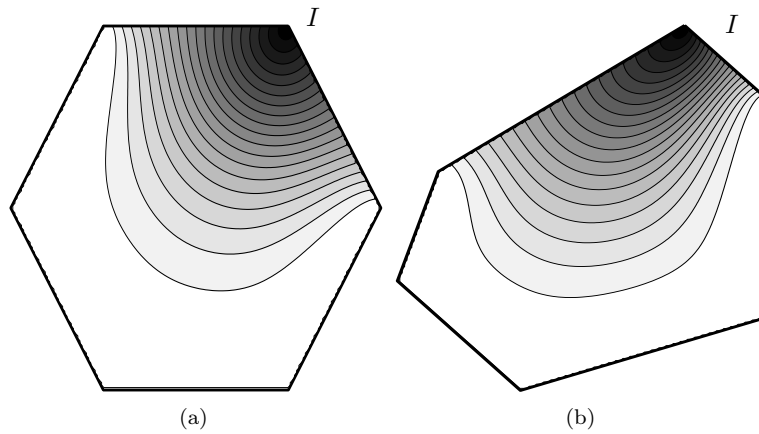


Figure 8: Laplace interpolant on a) canonical hexagonal domain b) Physical polygonal domain .

## 4 Linear Elasticity : Governing equations and weak form

We consider the displacement field  $\mathbf{u}(\mathbf{X})$  of a body described by an open bounded domain  $\Omega \subset \mathbb{R}^2$ , see Fig. 9.

On the Dirichlet boundary  $\Gamma_u$  the displacements  $\bar{\mathbf{u}}$  are given, whereas the Neumann boundary  $\Gamma_\sigma$  is loaded by the prescribed surface forces  $\bar{\mathbf{t}}$ . For small displacements, the governing equations are given by

$$\operatorname{div} \boldsymbol{\sigma} + \mathbf{b} = \mathbf{0} \quad \text{in } \Omega \quad (12a)$$

subjected to boundary conditions

$$\mathbf{u} = \bar{\mathbf{u}} \quad \text{on } \Gamma_u \quad (12b)$$

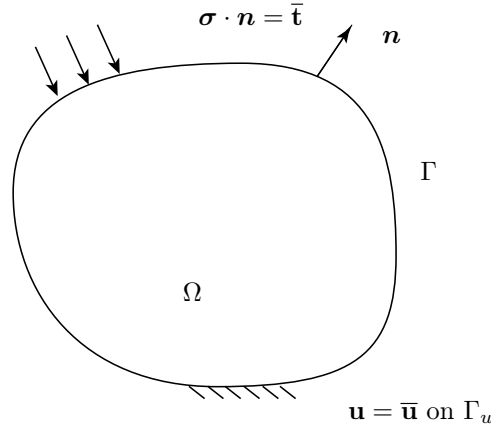


Figure 9: Two dimensional elastic body

$$\mathbf{t} = \boldsymbol{\sigma} \cdot \mathbf{n} = \bar{\mathbf{t}} \quad \text{on } \Gamma_\sigma \quad (12c)$$

with the body force per unit volume  $\mathbf{b}$  and the unit outward normal  $\mathbf{n}$  to  $\Gamma_\sigma$ .

The stress tensor for linear elasticity follows from  $\boldsymbol{\sigma} = \mathbf{D} : \boldsymbol{\varepsilon}$  with the strain tensor  $\boldsymbol{\varepsilon} = \frac{1}{2}[\nabla \mathbf{u} + \nabla^T \mathbf{u}]$  and the material moduli tensor  $\mathbf{D}$ . For a homogeneous isotropic material with the Navier-Lamé parameters  $\lambda$  and  $\mu$ , we obtain

$$\mathbf{D} = \lambda \mathbf{1} \otimes \mathbf{1} + 2\mu \mathbf{I}. \quad (13)$$

Where  $\mathbf{1}$  is the second order identity tensor and  $\mathbf{I}$  is the symmetric fourth order identity tensor. The weak form is consequently expressed as

$$\int_{\Omega} \boldsymbol{\sigma}(\mathbf{u}) : \boldsymbol{\varepsilon}(\boldsymbol{\eta}) \, d\Omega = \int_{\Omega} \mathbf{b} \cdot \boldsymbol{\eta} \, d\Omega + \int_{\Gamma} \bar{\mathbf{t}} \cdot \boldsymbol{\eta} \, d\Gamma. \quad (14)$$

For the discretization a displacement trial solution of the form  $\mathbf{u}^h \in V = [H^1(\Omega)]^2$  is chosen together with a set of kinematically admissible test functions  $\boldsymbol{\eta}^h \in V_0 = [H_0^1(\Omega)]^2$ , vanishing on the Dirichlet boundaries.

The trial and test functions are represented as linear combinations of  $C^0$  continuous interpolation functions,

$$\mathbf{u}^h(\mathbf{X}) = \sum_{I=1}^N \phi_I(\mathbf{X}) \mathbf{u}_I \quad \text{and} \quad \boldsymbol{\eta}^h(\mathbf{X}) = \sum_{I=1}^N \phi_I(\mathbf{X}) \boldsymbol{\eta}_I, \quad (15)$$

On substituting the trial and test functions and using the arbitrariness of nodal variations, the discrete system of linear equations

$$\mathbf{K} \mathbf{u} = \mathbf{f} \quad (16)$$

is obtained with the stiffness matrix

$$\mathbf{K} = \int_{\Omega^h} \mathbf{B}^T \mathbf{D} \mathbf{B} \, d\Omega^h \quad (17)$$

and the external load vector

$$\mathbf{f} = \int_{\Gamma^h} \boldsymbol{\phi}^T \bar{\mathbf{t}} \, d\Gamma^h + \int_{\Omega^h} \boldsymbol{\phi}^T \mathbf{b} \, d\Omega^h \quad (18)$$

where the matrix of the shape functions and the shape function derivatives are given by

$$\mathbf{B}_I = \begin{bmatrix} \phi_{I,X} & 0 \\ 0 & \phi_{I,Y} \\ \phi_{I,Y} & \phi_{I,X} \end{bmatrix}$$

and the material moduli tensor in Voigt notation for an isotropic linear material and plane stress condition reads

$$\mathbf{D} = \frac{E}{1-\nu^2} \begin{bmatrix} 1 & \nu & 0 \\ \nu & 1 & 0 \\ 0 & 0 & \frac{1-\nu}{2} \end{bmatrix}$$

## 5 Numerical integration of the weak form

Numerical integration of the Galerkin weak form is required to be performed over the polygonal domain for evaluating the integrals given in Eqn.(17) and Eqn.(18). The standard Gaussian integration rule is used for finite elements and for mesh free methods based on background cells. However for non polynomial type shape functions where barycentric coordinates are used, the Gaussian quadrature cannot guarantee exact results. Presently the state of the art includes the following methods for performing numerical integration over polygonal domains:

- Partitioning of the physical polygonal element domain  $\Omega$  into  $N$  triangular subdomains and performing numerical quadrature on the physical subdomains [16, 60],
- Partitioning of the canonical polygonal element domain  $\Omega_0$  into  $N$  triangular subdomains and performing numerical quadrature on the canonical subdomains with isoparametric mapping [60, 61],
- Cubature rules for irregular  $n$ -gons [62, 63] based on triangles [64, 65] or conformal mapping [11, 12],
- Generalized quadratures rules [66] on triangles or polygons based on symmetry groups and numerical optimization [14, 67–69].

In the present work we apply for simplicity the first two approaches and will apply our interpolants  $\phi_I$  for which in particular interpolation on physical elements is permitted. Any  $n$ -gonal domain may be decomposed into  $n$  pairwise disjoint triangular subdomains  $\bar{\Omega}$  and then any integration of a function  $\psi$  on a physical domain  $\Omega$  can be written as

$$\int_{\Omega} \psi \, d\Omega = \sum_n \int_{\bar{\Omega}} \psi \, d\bar{\Omega} \tag{19}$$

$$= \sum_n \int_{\bar{\Omega}_0} \psi |\mathbf{J}| \, d\bar{\Omega}_0 \tag{20}$$

$$= \sum_n \int_{\Omega_{\triangleleft}} \psi |\mathbf{J}| |\mathbf{J}_{\triangleleft}| \, d\bar{\eta} \, d\bar{\xi} \tag{21}$$

and thereby be pulled back for integration either on a triangle in the canonical domain  $\Omega_0$  or a generic triangular domain  $\Omega_{\triangleleft}$ . (19)-(21) may individually be integrated with any adequate quadrature scheme. We select classical 2d Gaussian quadrature defined on a generic triangular domain with  $n_{\triangleleft}^G$  quadrature points on each of the  $N$  subdomain triangles. For the application of (19) and (20) the Gauss points  $\mathbf{p}_{\triangleleft}^G$  and the associated weights  $w^G$  can also be mapped into the appropriate domains  $\Omega$  or  $\Omega_0$ , respectively.

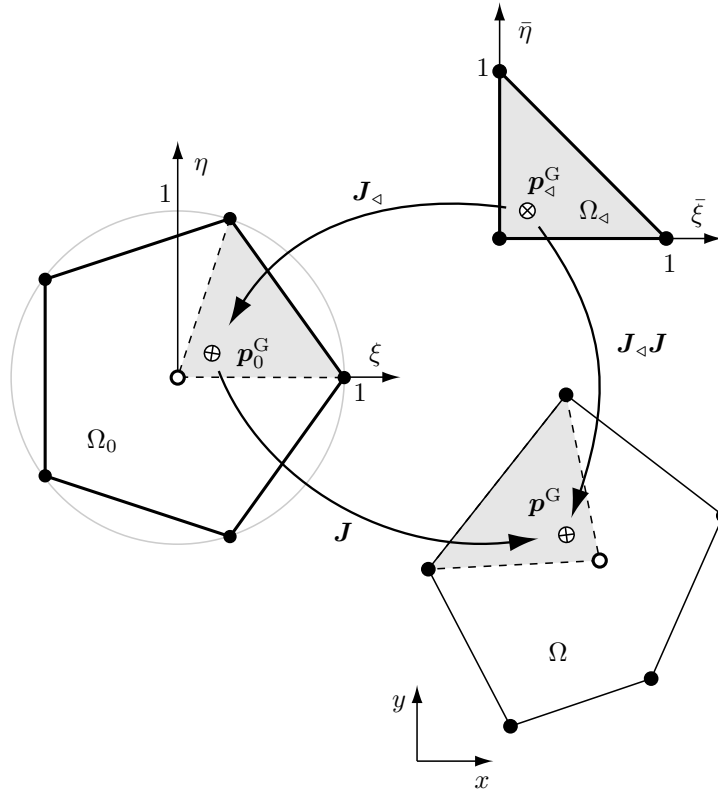


Figure 10: Numerical integration based on partition of the canonical  $\Omega_0$  or the physical element domain  $\Omega$  and mapping of quadrature points from a generic triangular domain  $\Omega_d$ .

## 6 Error estimation and Adaptivity

Adaptive techniques seek to construct reference solutions, define error norms and in general create a more accurate and reliable numerical solution by using a feed back strategy incorporating these reference solutions and error norms. *A - posteriori* estimates are more popular because of their robustness, they use the computed solution  $\mathbf{u}^h$  in order to determine an estimate of the form  $\|\mathbf{u} - \mathbf{u}^h\| \leq tol$  where *tol* is simply a number. These are also useful to perform adaptive mesh refinement.

### 6.1 *A-posteriori* error estimate

To assess the ability of polygonal finite elements to represent linear displacement fields, we first perform a displacement patch test. We use  $L^2(\Omega)$  and  $H^1(\Omega)$  norms of the displacement error to assess the performance of the polygonal finite element method. The  $L^2(\Omega)$  and  $H^1(\Omega)$  error norms are defined as follows

$$\|\mathbf{u} - \mathbf{u}^h\|_{L^2(\Omega)} = \sqrt{\int_{\Omega} [\mathbf{u} - \mathbf{u}^h]^T [\mathbf{u} - \mathbf{u}^h] d\Omega} \quad (22)$$

$$\|\mathbf{u} - \mathbf{u}^h\|_{H^1(\Omega)} = \|\mathbf{u} - \mathbf{u}^h\|_{L^2(\Omega)} + \sqrt{\int_{\Omega} [\nabla \mathbf{u} - \nabla \mathbf{u}^h]^T : [\nabla \mathbf{u} - \nabla \mathbf{u}^h] d\Omega}$$

where  $\mathbf{u}$  and  $\mathbf{u}^h$  are the exact and numerical displacements respectively.

In finite element methods, usually  $C^0$  (or  $C^1$  for some plate and shell elements) functions are used for the interpolation of the unknown function (i.e. displacements); this however entails a discontinuity in the derivatives across the element boundaries which gives rise to discretization errors. A post-processing procedure (for instance see [70], [71] and [41]) that uses these discontinuous derivatives to create smoothed functions in the error estimation process is then adopted. The discrepancy between element by element fields and smoothed fields serves as a measure of the discretization error. For this purpose, and then for deciding how the discretization can be improved, the smoothed field is regarded as the most accurate result the current mesh can provide. In the present work we use a *patch recovery* technique to obtain smoothed quantities.

The super convergent patch recovery technique was proposed by Zienkiewicz and Zhu ([43] and [42]). The basis of the method lies in the least square fit of an unknown polynomial over a patch of elements at sampling points. The smoothed stress field,  $\boldsymbol{\sigma}^\star$  over a patch can be written as,

$$\boldsymbol{\sigma}^\star = [P]\{a\} \quad (23)$$

Where  $[P]$  is the basis of an assumed polynomial, and  $\{a\}$  contains generalized co-ordinates to be determined. Different values of the  $a_i$  in  $\{a\}$  are obtained for different stress components. To determine  $\{a\}$  and thus define a smooth stress field, for the patch selected we sample the element stress field  $\boldsymbol{\sigma}$  at locations where it is likely to be most accurate and these points are generally Gauss points denoted as super convergent points. A least square fit of expansion Eqn.(23) to finite element solutions  $\boldsymbol{\sigma}$  obtained at sampling points over the patch is then made. Thus, we minimize the functional

$$\Pi = \sum_{j=1}^{nsp} [\boldsymbol{\sigma} - [P]\{a\}]^2 \quad (24)$$

where,  $nsp$  is the number of Gauss points in the patch. When  $\{a\}$  has been computed, the smoothed stress  $\boldsymbol{\sigma}^\star$  can be evaluated at any point inside the patch by substituting  $X$  and  $Y$  coordinates of the point in Eqn.(23).

The *global energy norm*  $\|U\|$  is defined as

$$\|U\| = \left[ \sum_{i=1}^m \int \{\boldsymbol{\sigma}\}_i^T \mathbb{D}^{-1} \{\boldsymbol{\sigma}\}_i d\Omega \right]^{\frac{1}{2}} \quad (25)$$

The corresponding error in the energy norm then follows as

$$\|e\| = \left[ \sum_{i=1}^m \int [ \{\boldsymbol{\sigma}\}_i^\star - \{\boldsymbol{\sigma}\}_i ]^T \mathbb{D}^{-1} [ \{\boldsymbol{\sigma}\}_i^\star - \{\boldsymbol{\sigma}\}_i ] d\Omega \right]^{\frac{1}{2}} \quad (26)$$

Where  $m$  is number of elements in the region of a structure whose error is to be estimated.

As an alternative to  $\|U\|$  and  $\|e\|$  one can work with  $L_2$  norm quantities. They are obtained from the foregoing expression by omitting the weighting matrix  $\mathbb{D}$ .

$$\|U\|_{L_2} = \left[ \sum_{i=1}^m \int \{\boldsymbol{\sigma}\}_i^T \{\boldsymbol{\sigma}\}_i d\Omega \right]^{\frac{1}{2}} \quad (27)$$

$$\|e\|_{L_2} = \left[ \sum_{i=1}^m \int [ \{\boldsymbol{\sigma}\}_i^\star - \{\boldsymbol{\sigma}\}_i ]^T [ \{\boldsymbol{\sigma}\}_i^\star - \{\boldsymbol{\sigma}\}_i ] d\Omega \right]^{\frac{1}{2}} \quad (28)$$

Where,  $\{\sigma^\star\}_i$  is the smooth stress field obtained from the *patch recovery* technique and  $\{\sigma\}_i$  are the finite element stresses. The relative error  $\eta$  used to quantify the discretization error over a patch of elements or the entire mesh, can then be defined as

$$\eta = \left[ \frac{\|e\|^2}{\|U\|^2 + \|e\|^2} \right]^{\frac{1}{2}} \quad (29)$$

The possible range of  $\eta$  is  $0 < \eta < 1$ .

## 6.2 Adaptive Meshing

The goal of adaptive meshing is to achieve a desired accuracy by refining a mesh where necessary and to coarsen where necessary in an iterative process. Automation of the process requires numerical indication on where and how to refine the discretization and a termination criteria. In our analysis we have used the *relative error norm*  $\eta$  described in Section 6.1, as a criteria for adaptivity.

A possible termination criteria is that the final value of  $\eta$  must not exceed an allowable value  $\eta_{all}$  in the final mesh. The average value of  $\|U\|^2 + \|e\|^2$  per element, in combination with  $\eta_{all}$ , provides an allowable value of error,  $\|e_i\|_{all}$  in an element. Thus from Eqn.(29), with  $m$  the number of elements in the mesh, the allowable error in a single element can be calculated as

$$\|e_i\|_{all} = \eta_{all} \left[ \frac{\|U\|^2 + \|e\|^2}{m} \right]^{\frac{1}{2}} \quad (30)$$

We then calculate  $\xi$  for each element, which is the ratio of the actual value of  $\|e_i\|$  in a typical element to the allowable value

$$\xi_i = \frac{\|e_i\|}{\|e_i\|_{all}} \quad (31)$$

The result  $\xi_i > 1$  indicates that more elements are needed in that location. After the first cycle, any element with  $\xi_i < 1$ , is ignored while attention is directed towards refinement of elements for which  $\xi_i > 1$ . With  $\chi_i$  a characteristic element dimension, the desired new size of the element  $i$  is taken as

$$(\chi_i)_{new} = \frac{(\chi_i)_{old}}{\xi_i} \quad (32)$$

In our work, the area of the element is considered as the characteristic element dimension  $\chi$ . Consider an initial coarse mesh as in Fig. 11(a) formed by the point set  $\mathcal{P}$ . Compute the finite element solution  $\sigma$  for this mesh and calculate the allowable error  $\|e_i\|_{all}$ , (Eqn.(30)) for each element in the mesh. Furthermore calculate  $\xi_i$  using Eqn.(31), for all the elements in the mesh. Fig.11(a) highlights the elements of the initial mesh with  $\xi > 1$ , indicating these elements need to be refined. For these elements we calculate  $(\chi_i)_{new}$ , as in Eqn.(32). To reduce the element size to  $(\chi_i)_{new}$ , extra seeds (say  $\mathcal{P}_i$ ) are randomly introduced in the erroneous elements where  $\xi_i > 1$ . The initial point set  $\mathcal{P}$  is updated with newly introduced seeds  $\mathcal{P}_i$  to get an updated point set,  $\mathcal{P}_{new}$ . The new mesh generated with this updated point set is shown in Fig. 11(b). This process is repeated until  $\eta < \eta_{all}$ . The steps in the iterative adaptive strategy are explained in algorithm 2.

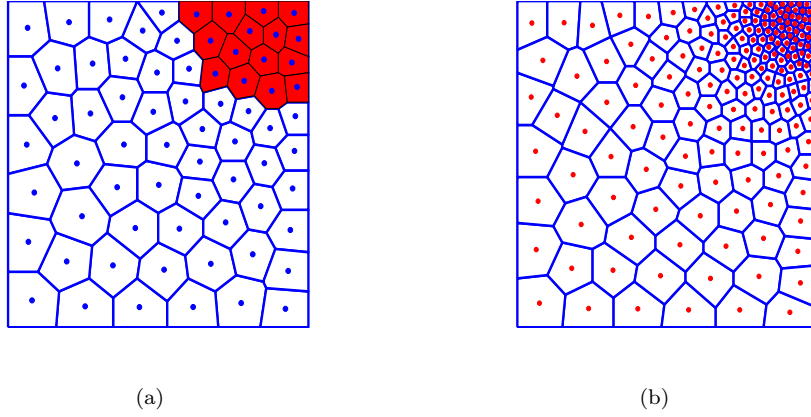


Figure 11: Adaptive refinement of a block. (a) Initial mesh with point set  $P_0$ , elements targeted for refinement with  $\xi_i > 1$  are marked in red. (b) Refined mesh with updated point set  $P_{new}$

---

**Algorithm 2** Algorithm for Adaptive strategy

---

- 1: Create an initial coarse mesh in  $\Omega$  with random initial point set  $\mathcal{P}$
  - 2: Compute the finite element solution  $\sigma$ .
  - 3: Compute the *relative error*  $\eta$  for the mesh as in Eqn.(29).
  - 4: **if**  $\eta > \eta_{all}$  **then**
  - 5: **for all** Elements **do**
  - 6: Compute *allowable error*  $\|e_i\|_{all}$  as in Eqn.(30).
  - 7: Compute  $\xi_i$  as in Eqn(31)
  - 8: **if**  $\xi_i > 1$  **then**
  - 9: Reduce the element size to  $(\chi_i)_{new}$  as in Eqn.(32) by introducing new set of random points  $\mathcal{P}_i$  in that element
  - 10: Update  $\mathcal{P}_{new} \leftarrow \mathcal{P} + \mathcal{P}_i$
  - 11: **end if**
  - 12: **end for**
  - 13: **end if**
  - 14: Generate new mesh with updated point set  $\mathcal{P}_{new}$
  - 15: Go to step 2
-

## 7 Numerical Examples

In this section, first we study the ability of the proposed method to represent a linear displacement field via the displacement patch test. Next the adaptive procedure given above is employed to refine the initial mesh, in order to get a desired mesh ( $\eta < \eta_{all}$ ). We consider three numerical examples under plane stress conditions to demonstrate the proposed method. Numerical integration on an  $n$ -sided polygon is performed using  $3 \times 3$  Gauss quadrature rule on  $n$ -sub-triangles of a  $n$ -sided polygon. In all the considered examples we use a modulus of elasticity  $E = 70000$  Mpa and Poisson's ratio,  $\nu = 0.3$ .

### 7.1 Displacement Patch test

As a first example, we study the ability of polygonal finite elements to represent linear displacement fields. We consider a unit square domain, as shown in Fig. 12. The test is performed by applying displacements of  $u_x = X_i$  and  $u_y = Y_i$  on the boundary nodes of a unit square domain. The displacement error norms,  $L_2$  and  $H_1$  are calculated for four different meshes shown in Fig.13. The values of  $L_2$  and  $H_1$  norms are tabulated in Table 1. The results reveal that the patch test is passed. The  $L_2$ -norm and  $H_1$ -norm of the displacement error are shown in Table 1.

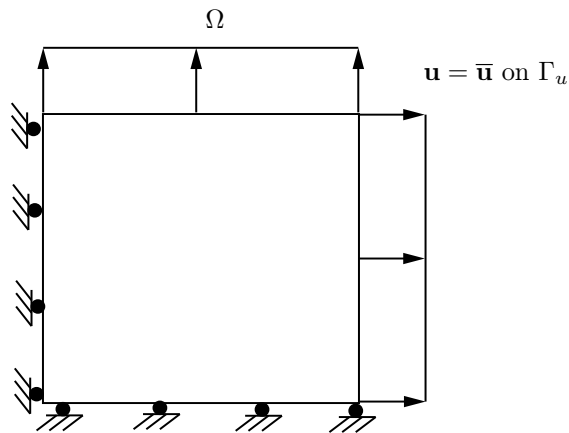


Figure 12: Unit square domain subjected to displacement field of  $u_x = X_i$  and  $u_y = Y_i$  on the boundary.

Table 1:  $L_2$  and  $H_1$  norm for displacement patch test

Mesh	$DOF$	$L_2$ norm	$H_1$ norm
a	42	2.21E-05	2.84E-04
b	82	1.62E-08	5.49E-06
c	160	1.53E-12	6.44E-08
d	318	9.74E-14	7.03E-12

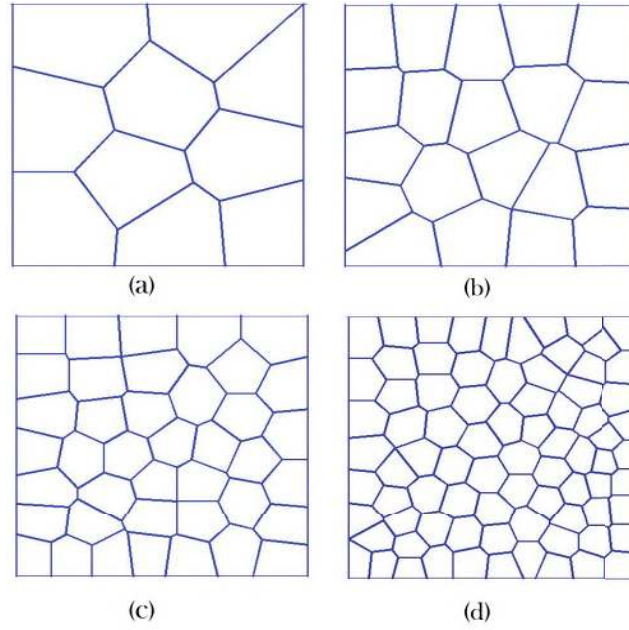


Figure 13: Different meshes considered for displacement patch test (a) Mesh with 10 elements,(b) Mesh with 20 elements,(c) Mesh with 40 elements,(d) Mesh with 80 elements.

## 7.2 Plate with a Circular hole

A non-convex plate with a traction-free circular hole is considered (edge length  $2\ell$ , hole radius  $a = \frac{\ell}{6}$ ). Fig.14 shows the quarter plate loaded by unidirectional tension  $\sigma_0 = 100$  Mpa in  $X$  - direction on the right edge. Due to symmetry, Dirichlet boundary conditions are imposed along  $AB(u_y = 0)$  and  $DE(u_x = 0)$ . In polar coordinates the exact stress field for an infinite plate with a hole is given by

$$\begin{aligned}
 \frac{\sigma_{xx}(r, \theta)}{\sigma_0} &= 1 - \frac{a^2}{r^2} \left[ \frac{3}{2} \cos 2\theta + \cos 4\theta \right] + \frac{3a^4}{2r^4} \cos 4\theta \\
 \frac{\sigma_{yy}(r, \theta)}{\sigma_0} &= -\frac{a^2}{r^2} \left[ \frac{1}{2} \cos 2\theta - \cos 4\theta \right] - \frac{3a^4}{2r^4} \cos 4\theta \\
 \frac{\sigma_{xy}(r, \theta)}{\sigma_0} &= -\frac{a^2}{r^2} \left[ \frac{1}{2} \sin 2\theta + \sin 4\theta \right] + \frac{3a^4}{2r^4} \sin 4\theta
 \end{aligned} \tag{33}$$

The corresponding displacement components are

$$\begin{aligned}
 u_x(r, \theta) &= \frac{a}{8\mu} \left[ \frac{r}{a} (\kappa + 1) \cos \theta + 2 \frac{a}{r} ((1 + \kappa) \cos \theta \right. \\
 &\quad \left. + \cos 3\theta) - 2 \frac{a^3}{r^3} \cos 3\theta \right]
 \end{aligned} \tag{34}$$

$$\begin{aligned}
 u_y(r, \theta) &= \frac{a}{8\mu} \left[ \frac{r}{a} (\kappa - 3) \sin \theta + 2 \frac{a}{r} ((1 - \kappa) \sin \theta \right. \\
 &\quad \left. + \sin 3\theta) - 2 \frac{a^3}{r^3} \sin 3\theta \right]
 \end{aligned} \tag{35}$$

with  $\kappa = 3 - 4\nu$ . In the numerical computations, we consider  $a = 10\text{mm}$ ,  $\ell = 60\text{mm}$  and the Laplace interpolant  $\phi_T^I$ . As a termination criteria we have chosen  $\eta_{all} = 5\%$ .

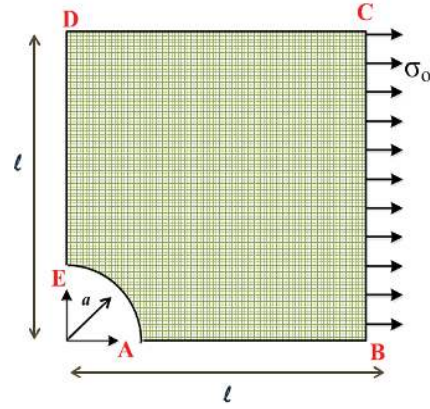


Figure 14: Quarter plate with circular hole under tension with symmetry axes

The initial discretization being the coarsest has 24 elements with 104 *DOF*. Following the procedure described earlier we perform an uniform and adaptive refinement on this initial coarse mesh. Fig. 16 and Fig. 17 show the different meshes obtained due to uniform and adaptive refinements respectively. Fig. 22 shows a plot of the relative error norm *vs* the number of degrees of freedom for the plate with hole example. It is seen in the graph that the initial coarse mesh having 104 degrees of freedom, has a  $\eta = 17.9\%$ . Adaptive refinement reaches the criteria of  $\eta < \eta_{all}$  (5% in this case) at 712 degrees of freedom, while it takes 1400 degrees of freedom for uniform refinement to satisfy the same criteria. We see that adaptive refinement converges at a relatively higher rate than uniform refinement. The stress plots for the plate with a hole example are shown in Fig. 18.

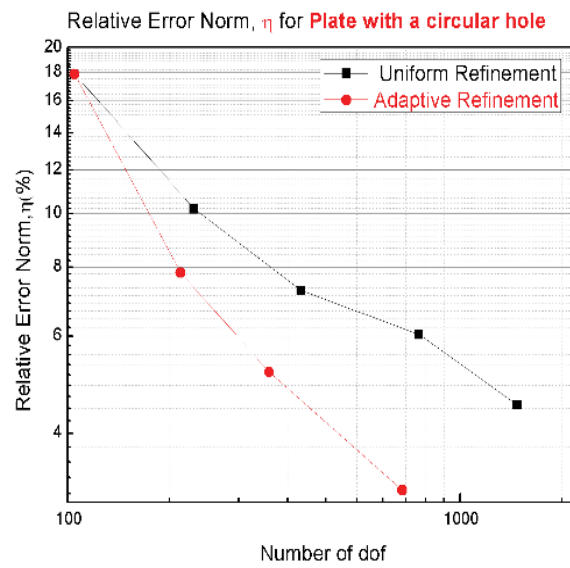


Figure 15: Plot of relative error norm  $\eta$  for Plate with a circular hole problem

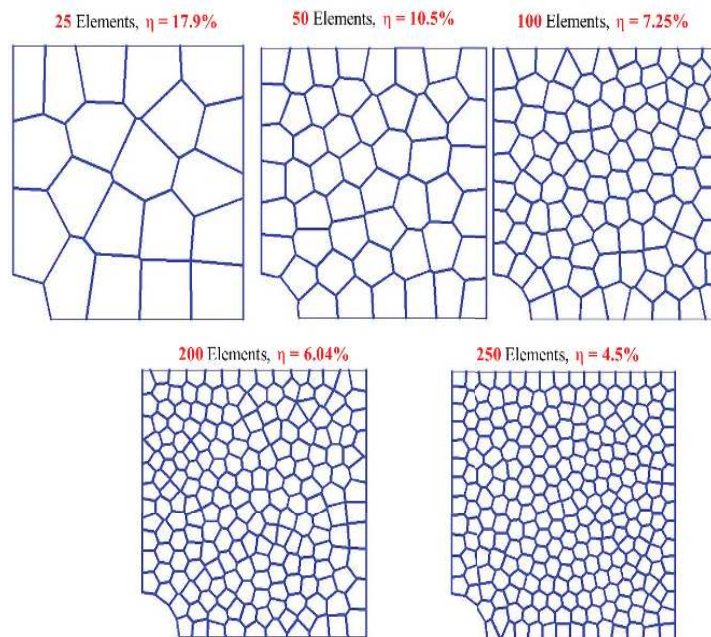


Figure 16: Meshes generated due to uniform refinement of the plate with a circular hole domain

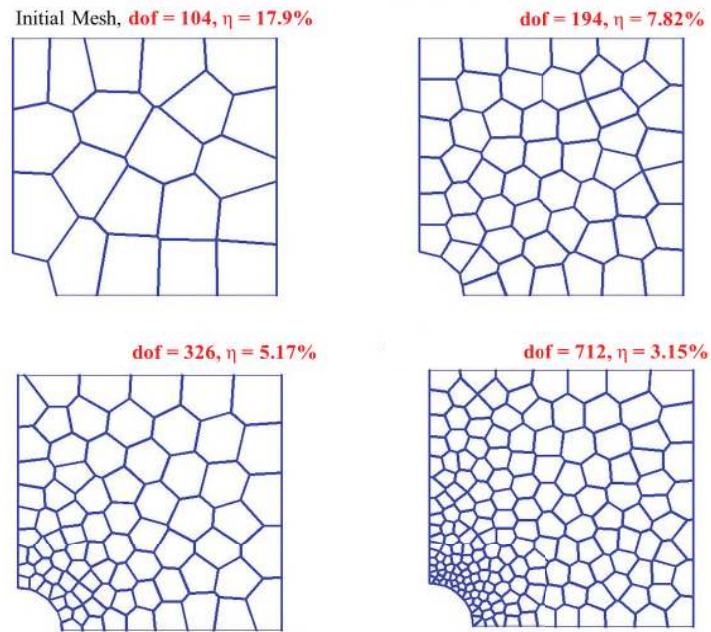


Figure 17: Meshes generated due to adaptive refinement of the plate with a circular hole domain

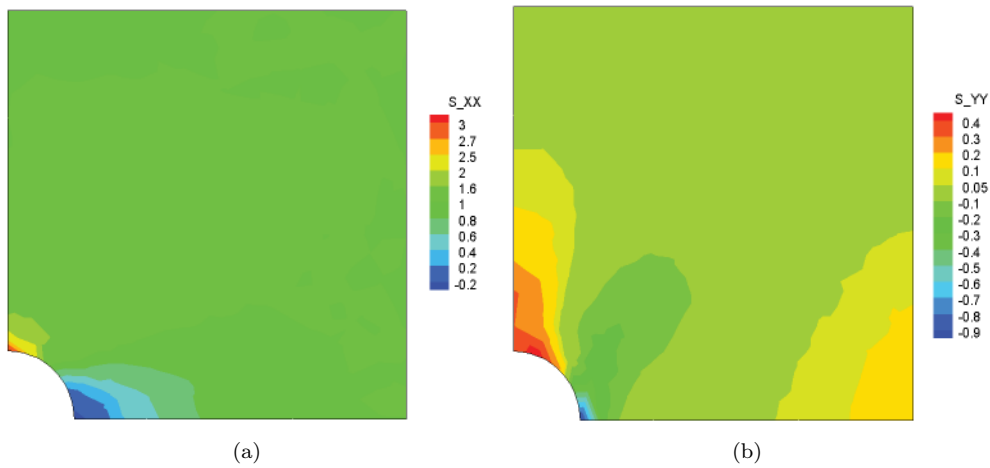


Figure 18: Stress plot for plate with a circular hole problem on the finest adaptive refined mesh. (a)  $\sigma_{xx}$   
(b)  $\sigma_{yy}$

### 7.3 L- shaped domain

A  $L$ -shaped specimen of the dimensions as shown in Fig. 20 is considered. The specimen is subjected to a prescribed displacement ( $u_x = 10mm$ ) and ( $u_y = 10mm$ ) along the two legs. To prevent rigid body motion all the deformation degrees of freedom at the re-entrant corner  $A$ , are additionally fixed. In the numerical computations we consider  $\ell = 100mm$  with the Laplace interpolant  $\phi_T^L$ . As a termination criteria we have chosen  $\eta_{all} = 10\%$ . The initial discretization being the coarsest has 25 elements in the domain with 108

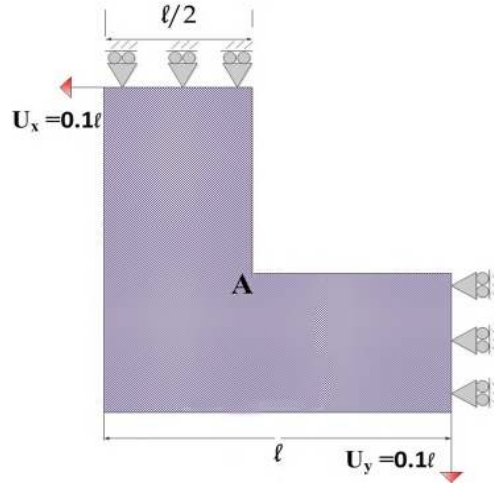


Figure 19:  $L$ -shaped specimen.

DOF. We perform uniform and adaptive refinement on this coarse mesh. Fig. 21 and Fig. 22 shows the different meshes obtained due to uniform and adaptive refinement. Fig.27 shows a plot of the relative error norm *vs* number of degrees of freedom for the  $L$ -shaped specimen example.

It is seen from the graph that the initial coarse mesh having 108 degrees of freedom, has an error of 29.7%. We also note that there is no much difference between the convergence rates of both the methods during the initial stages. This can be attributed to the fact that, initially most of the elements in the  $L$ -shaped domain are erroneous, i.e,  $\xi_i > 1$ , so that even in the adaptive refinement most of the elements are refined. After sufficiently many refinements, however, adaptive refinement steps off and reaches the criteria of  $\eta < \eta_{all}$  (10% in this case) at 2950 degrees of freedom, while even at 3000 degrees of freedom for the uniformly refined mesh the error is 13.2%, which is greater than  $\eta_{all}$ .

The stress plots for the  $L$  shaped domain example for the finest adaptive mesh are shown in Fig.23.

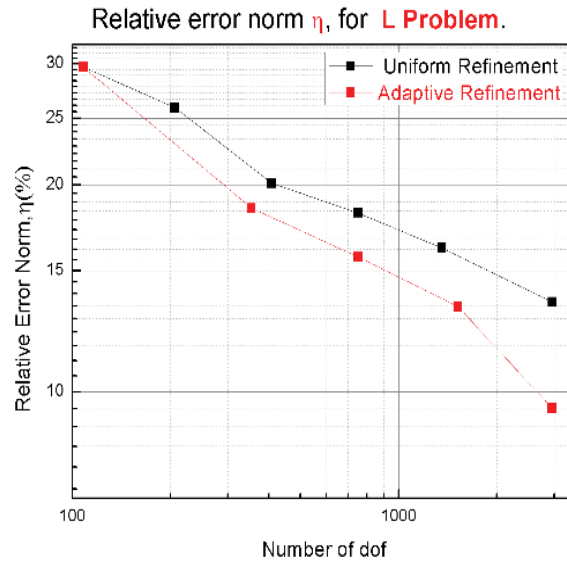


Figure 20: Plot of relative error norm  $\eta$  for L shaped domain problem.

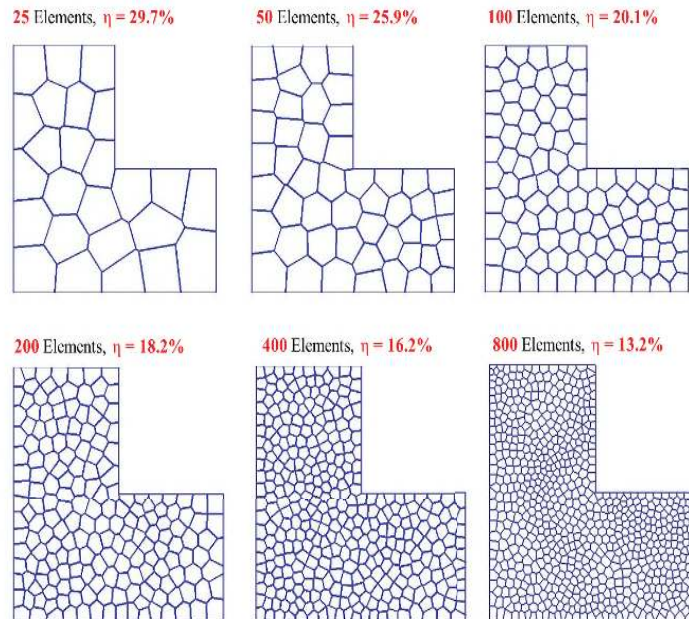


Figure 21: Meshes generated due to uniform refinement of  $L$  shaped domain.

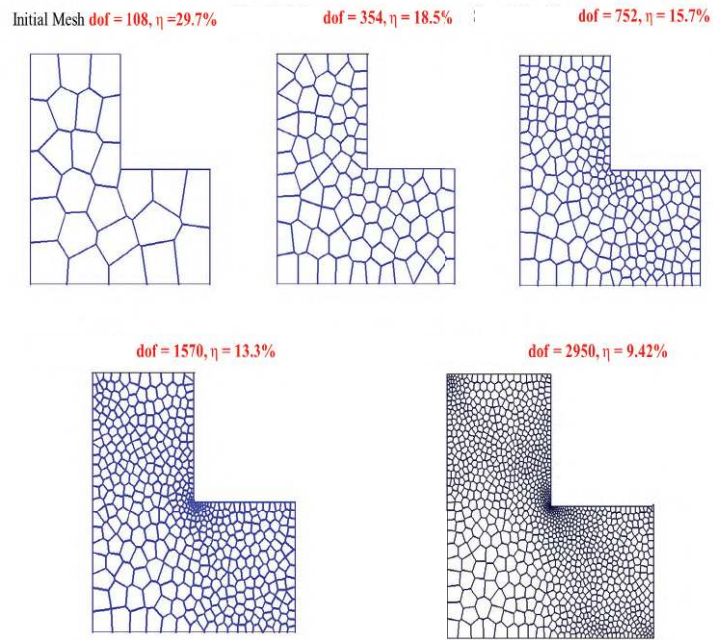


Figure 22: Meshes generated due to adaptive refinement of  $L$ -shaped domain

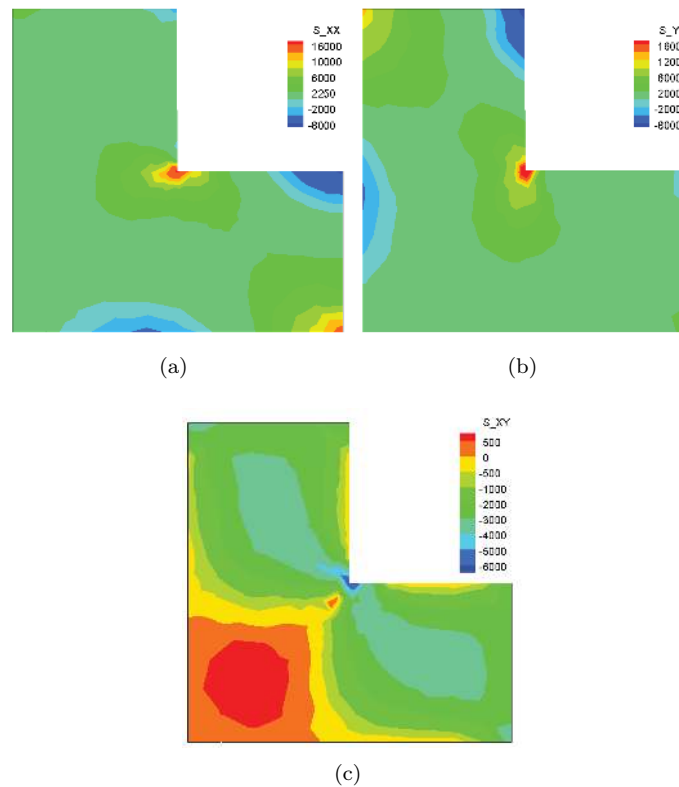


Figure 23: Stress plot for  $L$ -shaped domain problem for the finest adaptive mesh.

#### 7.4 Bracket problem

As a last example we consider a mechanical connection as shown in Fig 25. The bracket has 2 bolt holes and all degrees of freedom along the bolt holes are restrained and are subjected to 2 point loads at the tips. In the numerical computations, we consider  $\ell = 100mm$ ,  $a = 50mm$  and bolt holes of diameter  $25mm$ , i.e,  $b = 12.5mm$ ,  $P = 500N$  with the Laplace interpolant  $\phi_I^T$ . As a termination criteria we have chosen  $\eta_{all} = 15\%$ .

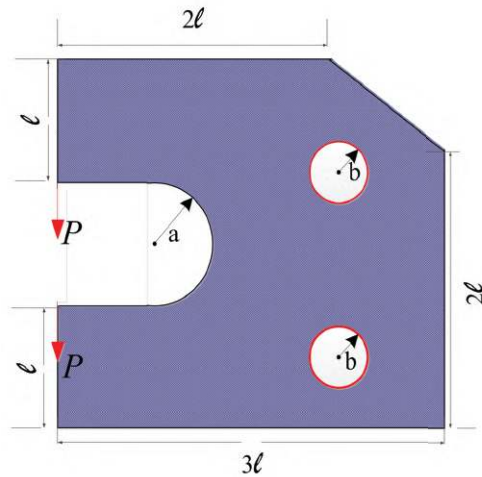


Figure 24: Mechanical connection.

The initial discretization being the coarsest has 29 elements with 118 DOF. We perform uniform and adaptive refinement on this mesh. Fig. 26 and Fig. 27 show the different meshes obtained due to uniform and adaptive refinement, respectively.

Fig. 25 shows a plot of the relative error norm *vs* the number of degrees of freedom for the bracket example. It is seen from the graph that the initial coarse mesh having 108 degrees of freedom has an error of 49.7%. We can observe from the graph that the criteria of  $\eta < \eta_{all}$  (15% in this case) is achieved at 3070 degrees of freedom with adaptive refinement, while even at 3900 degrees of freedom the uniformly refined mesh possesses an error of 17.8%, which is greater than  $\eta_{all}$ . The stress plots for the bracket problem for the finest adaptive mesh are shown in Fig. 28.

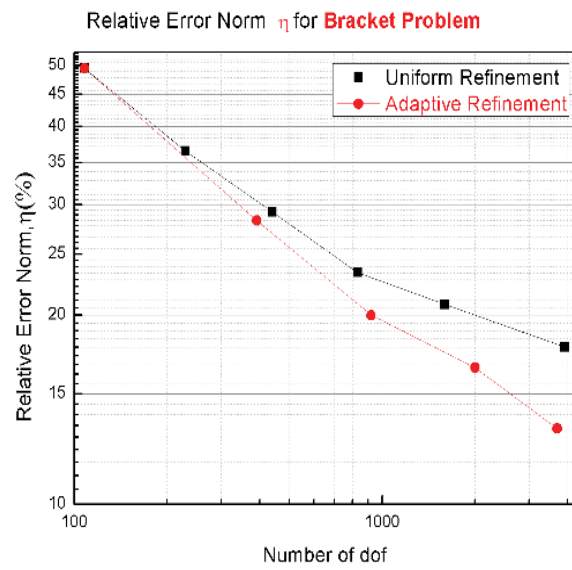
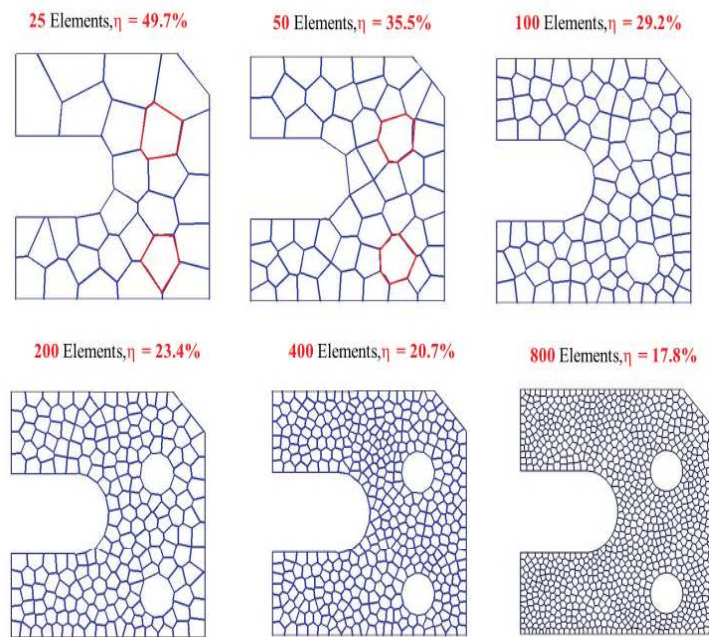
Figure 25: Plot of relative error norm  $\eta$  for Bracket problem.

Figure 26: Meshes generated due to uniform refinement of bracket domain.

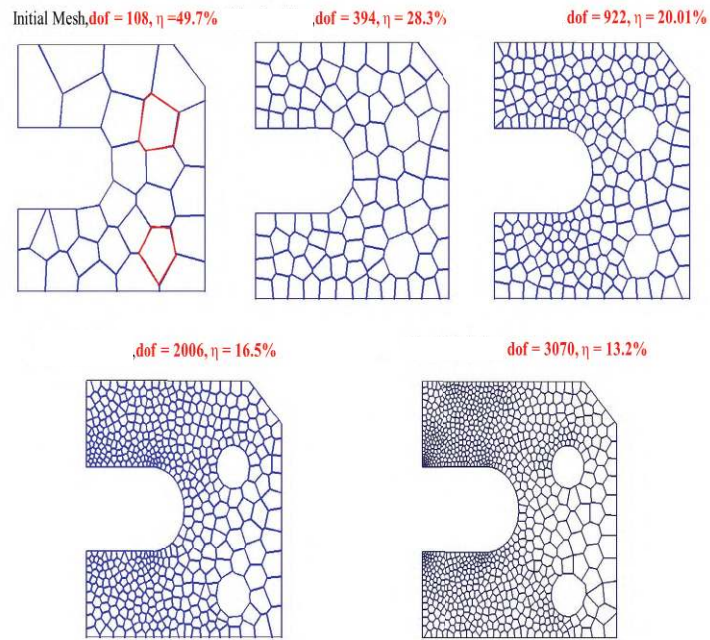


Figure 27: Meshes generated due to adaptive refinement of bracket domain.

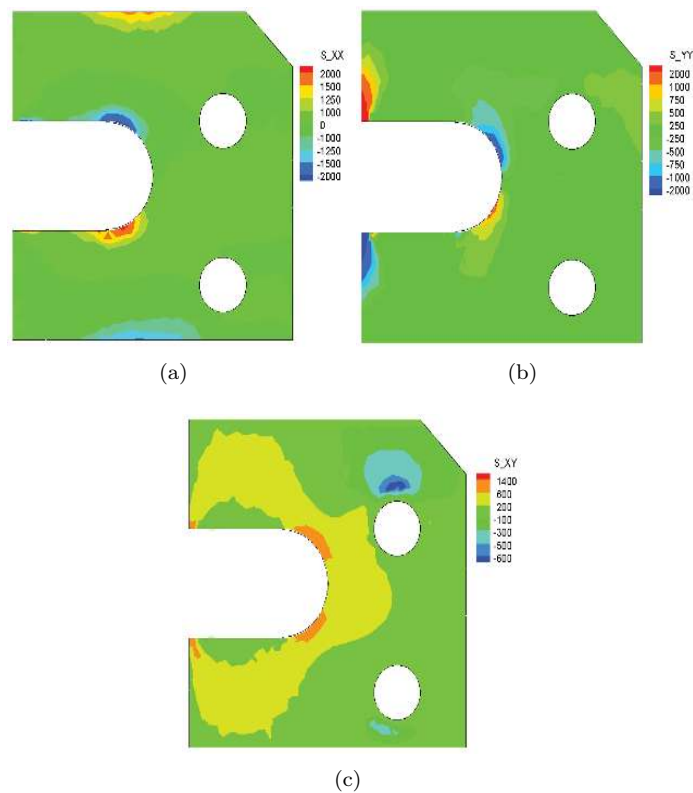


Figure 28: Stress plot for bracket problem for the finest adaptive mesh.

## 8 Conclusions

In this work we presented an adaptive polygonal finite element method (Poly-FEM) for the analysis of two dimensional plane elasticity problems. The generation of the polygonal finite element mesh is based on the generation of a centroidal Voronoi tessellation (CVT). The method has been extended to include tessellations for non-convex domains. In this work we have implemented a region by region adaptive polygonal element mesh generation. A patch recovery type of stress smoothing technique that utilizes polygonal element patches for obtaining smooth stresses has been proposed. A recovery type *a-posteriori* error estimator that shows the energy norm of the error from the recovered solution is then computed for the polygonal finite element method. The refinement of the polygonal elements is made on a region by region basis through a refinement index. For the numerical integration of the Galerkin weak form over polygonal finite element domains, we resort to classical Gaussian quadrature applied on triangular sub-domains of each polygonal element. Numerical examples of two dimensional plane elasticity problems are presented to demonstrate the efficiency of the proposed adaptive polygonal finite element method. It is clearly seen from the trends in the numerical results that the proposed adaptive polygonal FEM results in flexible discretization, with less number of degrees of freedom than uniform refinement. The convergence characteristics indicate reduced error norms when compared to uniform refinement together with faster rates of convergence.

## 9 Acknowledgement

The last author acknowledges support by the cluster of excellence "Engineering of Advanced Materials"

## References

- [1] K. Y. Sze and N. Sheng, "Polygonal finite element method for nonlinear constitutive modeling of polycrystalline ferroelectrics," *Finite Elements in Analysis and Design*, vol. 42, pp. 107–129, 2005.
- [2] A. Jayabal, K. Menzel and A. Arockiarajan, "Micromechanical modelling of switching phenomena in polycrystalline piezoceramics: application of polygonal finite element approach.," *Computational Mechanics*, vol. 48, pp. 421–435, 2011.
- [3] C. R. Dohrmann, W. K. Samuel, and M. W. Heinstein, "A method for connecting dissimilar finite element meshes in two dimensions," *International Journal for Numerical Methods in Engineering*, vol. 48, pp. 655–678, 2000.
- [4] Y. A. Kuznetsov, "Mixed finite element method for diffusion equations on polygonal meshes with mixed cells," *Journal of Numerical Mathematics*, vol. 14, pp. 305–315, 2006.
- [5] M. M. Rashid and P. M. Gullett, "On a finite element method with variable element topology," *Computational Methods in Applied Mechanics and Engineering*, vol. 190, pp. 1509–1527, 2000.
- [6] K. Y. Dai, G. R. Liu, and T. T. Nguyen, "An n-sided polygonal smoothed finite element method (nSFEM) for solid mechanics.," *Finite Elements in Analysis and Design*, vol. 43, pp. 847–860, 2007.
- [7] C. Talischi, G. Paulino, A. Pereira, and I. Menezes, "Polygonal finite elements for topology optimization: A unifying paradigm," *International Journal for Numerical Methods in Engineering*, vol. 82, pp. 671–698, 2010.
- [8] B. Lin and S. N. Chandlerwilde, "Numerical conformal mapping and mesh generation for polygonal and multiply connected regions," *Journal of Hydroinformatics*, vol. 2, pp. 255–266, 2000.

- [9] T. Nguyen-Thoi, G. R. Liu, and H. Nguyen-Xuan, “An n-sided polygonal edge - based smoothed finite element method (nES-FEM) for solid mechanics.,” *International Journal for Numerical methods in Biomedical Engineering*, vol. 27, pp. 1446–1472, 2010.
- [10] M. Kraus, A. Rajagopal, and P. Steinmann, “Investigations on polygonal finite element method : constrained adaptive Delaunay tessellation and conformal interpolants,” *Computers and Structures*, vol. 120, pp. 33–46, 2013.
- [11] S. Natarajan, S. Bordas, and D. R. Mahapatra, “Numerical integration over arbitrary polygonal domains based on Schwarz-Christoffel conformal mapping,” *International Journal for Numerical Methods in Engineering*, vol. 80, pp. 103–134, 2009.
- [12] S. Natarajan, S. Bordas, and D. R. Mahapatra, “Integrating strong and weak discontinuities without integration sub cells and example applications in XFEM/GFEM framework,” *International Journal for Numerical Methods in Engineering*, vol. 83, pp. 269–294, 2010.
- [13] C. J. Li, P. Lamberti, and C. Dagnino, “Numerical integration over polygons using an eight-node quadrilateral spline finite element.,” *Journal of Computational and Applied Mathematics*, vol. 233, pp. 279–292, 2009.
- [14] S. E. Mousavi, H. Xiao, and N. Sukumar, “Generalized gaussian quadrature rules on arbitrary polygons,” *International Journal of Numerical Methods in Engineering*, vol. 82, pp. 99–113, 2009.
- [15] J. Yvonnet, D. Ryckelynck, P. Lorong, and F. Chinesta, “A new extension of the natural element method for non-convex and discontinuous problems: the constrained natural element method (C-NEM),” *International Journal for Numerical Methods in Engineering*, vol. 60, no. 8, pp. 1451–1474, 2004.
- [16] A. Constantiniu, P. Steinmann, T. Bobach, G. Farin, and G. Umlauf, “The adaptive Delaunay tessellation: a neighborhood covering meshing technique,” *Computational Mechanics*, vol. 42, pp. 655–669, 2008.
- [17] N. Sukumar and A. Manzini, G. and Russo, “Hourglass stabilization and the virtual element method,” *International Journal for Numerical Methods in Engineering*, vol. 1, pp. 1–33, 2000.
- [18] H. Chi, C. Talischi, L. P. Oscar, and G. H. Paulino, “Polygonal finite elements for finite elasticity,” *International Journal for Numerical Methods in Engineering*, vol. 101, pp. 305–328, 2015.
- [19] G. Manzini, A. Russo, and N. Sukumar, “New perspectives on polygonal and polyhedral finite element methods,” *Mathematical Models and Methods in Applied Sciences*, vol. 24, no. 8, pp. 1665–1699, 2014.
- [20] G. Manzini, A. Russo, and N. Sukumar, “Gradient bounds for Wachspress coordinates on polytopes,” *SIAM Journal of Numerical Analysis*, vol. 52, no. 1, pp. 515–532, 2014.
- [21] C. Talischi, A. Pereira, G. H. Paulino, I. F. M. Menezes, and M. S. Carvalho, “Polygonal finite elements for incompressible fluid flow,” *International Journal for Numerical Methods in Fluids*, vol. 74, no. 2, pp. 134–151, 2014.
- [22] L. G. Arun, C. Talischi, and G. H. Paulino, “On the virtual element method for three-dimensional linear elasticity problems on arbitrary polyhedral meshes,” *Computer Methods in Applied Mechanics and Engineering*, vol. 282, pp. 132–160, 2014.
- [23] S. O. R. Biabanaki and A. R. Khoei, “A polygonal finite element method for modeling arbitrary interfaces in large deformation problems,” *Computational Mechanics*, vol. 50, pp. 19–33, 2012.

- [24] S. O. R. Biabanaki, A. R. Khoei, and P. Wriggers, “Polygonal finite element methods for contact-impact problems on non-conformal meshes,” *Computer Methods in Applied Mechanics and Engineering*, vol. 269, pp. 198–221, 2014.
- [25] N. Sukumar, “Quadratic maximum-entropy serendipity shape functions for arbitrary planar polygons,” *Computational Methods in Applied Mechanics and Engineering*, vol. 263, pp. 27–41, 2013.
- [26] T. Nguyen Thoi, H. Nguyen Xuan, P. Phung Van, T. Rabczuk, and C. Le Van, “Free and forced vibration analysis using the n-sided polygonal cell-based smoothed finite element method (ncs-fem),” *International Journal of Computational Methods*, vol. 10, no. 1, pp. 1–19, 2013.
- [27] K. Hornmann and N. Sukumar, “Maximum entropy coordinates for arbitrary polytopes,” *Eurographics Symposium on Geometry Processing 2008*, vol. 27, no. 5, pp. 1–12, 2009.
- [28] C. David and H. K. Nancy, “Generation of polyhedral delaunay meshes,” *Procedia Engineering*, vol. 82, pp. 291–300, 2014.
- [29] P. Yijiang, Z. Lijuan, P. Jiwei, and G. Qing, “A two-dimensional base force element method using concave polygonal mesh,” *Engineering Analysis with Boundary Elements*, vol. 42, pp. 45–50, 2014.
- [30] M. Kraus and P. Steinmann, “Finite element formulations for 3D convex polyhedra in nonlinear continuum mechanics,” *Computer Assisted Methods in Engineering and Sciences*, vol. 19, pp. 121–134, 2012.
- [31] S. Gosh and S. Moorthy, “Elastic plastic analysis of arbitrary heterogeneous materials with the Voronoi cell finite element method,” *Computer Methods in Applied Mechanics and Engineering*, vol. 121, no. 1–4, pp. 373–409, 1995.
- [32] H. W. Zhang, H. Wang, B. S. Chen, and Z. Q. Xie, “Analysis of Cosserat materials with Voronoi cell finite element method and parametric variational principle,” *Computer Methods in Applied Mechanics and Engineering*, vol. 197, no. 6–8, pp. 741–755, 2008.
- [33] S. Natarajan, E. T. Ooi, I. Chiong, and C. Song, “Convergence and accuracy of displacement based finite element formulations over arbitrary polygons: laplace interpolants, strain smoothing and scaled boundary polygon formulation,” *Finite Elements in Analysis and Design*, vol. 85, pp. 101–122, 2014.
- [34] A. R. Andrew Gillette and C. Bajaj, “Error estimates for generalized barycentric interpolation,” *Advances in Computational Mathematics*, vol. 37, no. 3, pp. 417–439, 2012.
- [35] W. Chunmei and W. Junping, “An efficient numerical scheme for the biharmonic equation by weak galerkin finite element methods on polygonal or polyhedral meshes,” *Computers and Mathematics with Applications*, vol. 68, no. 12, pp. 2314–2330, 2014.
- [36] S. Rjasanow and S. Weiber, “Higher order BEM-based FEM on polygonal meshes,” *Society for Industrial and Applied Mathematics*, vol. 50, no. 5, pp. 2357–2378, 2012.
- [37] F. J. Sayas, “The validity of johnson–nedelec’s BEM–FEM coupling on polygonal interfaces,” *Society for Industrial and Applied Mathematics*, vol. 55, no. 1, pp. 131–146, 2013.
- [38] I. Babuska and A. Aziz, “The mathematical foundation of the finite element method with applications to partial differential equations,” *Academic Press, New York*, 1972.
- [39] I. Babuska and W. C. Rheinboldt, “A-posteriori error estimates for the finite element method,” *International Journal for Numerical Methods in Engineering*, vol. 12, pp. 1597–1615, 1978.

- [40] I. Babuska and A. Miller, “A feedback finite element method with a posteriori error estimation: Part I. the finite element method and some basic properties of the a posteriori error estimator,” *Computer Methods in Applied Mechanics and Engineering*, vol. 61, pp. 1–40, 1987.
- [41] O. C. Zienkiewicz and E. Rank, “A simple error estimator in finite element method,” *Communications in Applied Numerical Methods*, vol. 3, pp. 243–249, 1987.
- [42] O. Zienkiewicz and J. Zhu, “The superconvergent patch recovery and a posteriori error estimates part 2: Error estimates and adaptivity,” *International Journal for Numerical Methods in Engineering*, vol. 33, no. 7, pp. 1365–1382, 1992.
- [43] O. Zienkiewicz and J. Zhu, “The superconvergent patch recovery and a posteriori error estimates part I: The recovery technique,” *International Journal for Numerical Methods in Engineering*, vol. 33, no. 7, pp. 1331–1364, 1992.
- [44] E. Stein, M. Ruter, and O. Stephan, “Error-controlled adaptive goal-oriented modeling and finite element approximations in elasticity,” *Computer Methods in Applied Mechanics and Engineering*, vol. 196, no. 2, pp. 3598–3613, 2007.
- [45] J. T. Oden and S. Prudhomme, “Goal-oriented error estimation and adaptivity for the finite element method,” *International Journal of Computers and mathematics*, vol. 41, no. 2, pp. 735–756, 1999.
- [46] P. M. Mohite and C. S. Upadhyay, “Focussed adaptivity for laminate plates,” *International Journal of Computers and Structures*, vol. 81, no. 2, pp. 287–298, 2003.
- [47] A. Rajagopal and S. Sivakumar, “An r-h adaptive strategy for analysis of plane problems with bimaterial interfaces,” *Computational Mechanics*, vol. 41, no. 1, pp. 49–72, 2007.
- [48] J. Mackerle, “Error estimates and adaptive finite element methods- a bibliography (1990-2000).,” *Engineering Computations*, vol. 18(5/6), pp. 802–914, 2001.
- [49] J. O. Dow, “A unified approach to finite element method and error analysis procedure,” *Academic Press, New York*, 1999.
- [50] R. Denzer, M. Scherer, and P. Steinmann, “An adaptive singular finite element in nonlinear fracture mechanics,” *Defect and Material Mechanics, C Dascalu, G A Maugin, C Stolz (eds)*, pp. 181–190, 2008.
- [51] J. Friederich, G. Leugering, and P. Steinmann, “Adaptive refinement based on asymptotic expansions of finite element solution for node insertion in 1d,” *GAMM-Mitteilungen*, vol. 35, no. 2, pp. 175–190, 2012.
- [52] A. Gillette, A. Rand, and P. Bajaj, “Error estimates for generalized barycentric interpolation,” *Advanced Computational Mathematics*, vol. 37, pp. 417–439, 2012.
- [53] O. Gonzalez Estrada, E. Nadal, J. Rodenas, P. Kerfriden, S. A. Bordas, and F. J. Fuenmayor, “Mesh adaptivity driven by goal oriented locally equilibrated superconvergent patch recovery,” *Computational Mechanics*, vol. 53, pp. 957–976, 2014.
- [54] X. Gan and J. E. Akin, “Super convergent second derivative recovery for lower order strain gradient plasticity,” *Computers and Structures*, vol. 135, pp. 118–127, 2014.
- [55] C. Talischi, G. H. Paulino, A. Pereira, and I. F. M. Menezes, “Polymesher: a general purpose mesh generator for polygonal elements in matlab,” *Structural and Multidisciplinary Optimization*, vol. 45, pp. 309–328, 2012.

- [56] V. V. Belikov, V. D. Ivanov, V. K. Kontorovich, S. A. Korytnik, and A. Y. Semenov, “The non-Sibson interpolation: A new method of interpolation of the values of a function on an arbitrary set of points,” *Computational Mathematics and Mathematical Physics*, vol. 37, pp. 9–15, 1997.
- [57] N. H. Christ, R. Friedberg, and T. D. Lee, “Weights of links and plaquettes in a random lattice,” *Nuclear Physics B*, vol. 210, pp. 337–346, 1982.
- [58] H. Hiyoshi and K. Sugihara, “Two generalizations of an interpolant based on Voronoi diagrams,” *International Journal of Shape Modeling*, vol. 5, pp. 219–231, 1999.
- [59] R. Sibson, “A vector identity for the Dirichlet tessellation,” *Mathematical Proceedings of Cambridge Philosophical Society*, vol. 87, pp. 151–155, 1980.
- [60] N. Sukumar and A. Tabarraei, “Conforming polygonal finite elements,” *International Journal for Numerical Methods in Engineering*, vol. 61, pp. 2045–2066, 2004.
- [61] G. Dasgupta, “Integration within polygonal finite elements,” *Journal of Aerospace Engineering*, vol. 16, pp. 9–18, 2003.
- [62] S. De and K. J. Bathe, “The method of finite spheres,” *Computational Mechanics*, vol. 25, pp. 329–345, 2000.
- [63] S. De and K. J. Bathe, “The method of finite spheres with improved numerical integration,” *Computers and Structures*, vol. 79, pp. 2183–2196, 2001.
- [64] M. A. Taylor, “Asymmetric cubature formulas for polynomial integration in the triangle and square,” *Journal of Computational and Applied Mathematics*, vol. 218, pp. 184–191, 2008.
- [65] S. Wandzura and H. Xiao, “Symmetric quadrature rules on a triangle,” *Computers and Mathematics with Applications*, vol. 45, pp. 1829–1840, 2003.
- [66] J. Ma, V. Rokhlin, and S. Wandzura, “Generalized quadrature of systems of arbitrary functions,” *Society of Industrial and Applied Mathematics*, vol. 33, pp. 971–996, 1996.
- [67] P. Silvester, “Symmetric quadrature formula for simplexes,” *Mathematics of Computation*, vol. 24, pp. 95–100, 1970.
- [68] J. N. Lyness and D. Jespersen, “Moderate degree symmetric quadrature rule for triangles,” *IMA Journal of Applied Mathematics*, vol. 15, pp. 19–32, 1975.
- [69] H. Xiao and Z. Gimbutas, “A numerical algorithm for construction of efficient quadrature rules in two and higher dimensions,” *Computers and Mathematics with Applications*, vol. 59, no. 2, pp. 663–676, 2010.
- [70] E. Hinton and J. S. Campbell, “Local and global smoothing of discontinuous finite element functions using a least squares method,” *International Journal for Numerical Methods in Engineering*, vol. 8, no. 3, pp. 461–480, 1974.
- [71] J. T. Oden and H. J. Brauchil, “On the calculation of consistent stress distributions in finite element approximations,” *International Journal for Numerical methods in Engineering*, vol. 3, pp. 317–325, 1971.